Kim et al., Environmental Research Letters (2018) **Supplementary materials**

Supplementary Data and Method

Text S1. The AMSR-E and AMSR2 Tb data merging method

The NASA Advanced Microwave Scanning Radiometer for EOS (AMSR-E) sensor was operational from June 2002 to October 2011. The AMSR-E microwave sensor provided twice-daily global brightness temperature (T_b) observations with sensor descending/ascending orbital equatorial crossings at 1:30 AM/PM local time, allowing day and night monitoring. After the loss of AMSR-E operations on October 4 2011, the Advanced Microwave Scanning Radiometer 2 (AMSR2) sensor was launched on May 18, 2012 on the Japan Aerospace Exploration Agency (JAXA) GCOM-W1 satellite. AMSR2 is similar to AMSR-E in sensor configuration, including microwave frequencies, sensor incidence angles and orbital equatorial crossing times. The AMSR-E 36.5 GHz orbital swath T_b data have a native footprint resolution of 14km x 8km (Kawanishi et al., 2003), while the similar frequency T_b orbital swath (L1R) data from AMSR2 has a native 12km x 7km footprint resolution (Imaoka et al., 2010). These data were merged by resampling the T_b records to a consistent 6 km polar EASE-Grid 2 projection format (Brodzik et al., 2014) using an inverse distance squared weighting interpolation method (Du et al., 2017).

Text S2. Modified seasonal threshold algorithm (MSTA)

The MSTA approach used to construct the AMSR FT record assumes that the large changes in microwave dielectric constant of the land surface that occur around the 0°C temperature threshold are associated with landscape FT transitions that dominate the corresponding satellite 36.5 GHz T_b seasonal dynamics, rather than other potential sources of T_b variability (Kim et al., 2011, 2017a). The MSTA classifies daily T_b variations in relation to grid cell-wise FT thresholds calibrated using ancillary 6-km resolution surface air temperature maps downscaled from coarser (0.25 degree) resolution ERA-Interim global reanalysis daily surface meteorological data (Dee et al., 2011). The 0.25 degree resolution ERA-Interim temperatures were spatially downscaled to the AMSR 6-km polar grid using a digital elevation map (DEM; Hasting et al., 1999) and annual mean environmental lapse rates derived from per grid cell linear regression relationships between the DEM elevations and MODIS Aqua land surface temperatures (Kim et al., 2017b). A 0.0°C temperature threshold was used in the MSTA to define the T_b based FT threshold between predominantly frozen and non-frozen landscape conditions within a grid cell.

The AMSR 36.5 GHz frequency T_b retrievals are not directly sensitive to near surface air temperatures, but rather the frequency dependent dielectric changes associated with shifts in the relative abundance of liquid water at the land surface that occur during FT transitions (Andre et al., 2015; Bateni et al., 2013; Holmes et al., 2013). The resulting AMSR FT data

record is available in a 6-km resolution polar EASE-grid 2 projection format for the ABR domain (Kim et al., 2018). The mean annual FT spatial classification agreement for the 15-year AMSR FT record (2002-2016) was 93.0±0.4 [inter-annual SD] percent and 85.9±0.9 [inter-annual SD] percent for the respective PM and AM overpasses, as derived from daily grid cell-to-point comparisons against *in situ* surface air temperature measurement based FT observations (based on a FT threshold of 0°C) from 4829±455 [inter-annual SD] ABR weather stations (Kim et al. 2018). The FT data quality metrics include detailed data quality (QC) flags and other documentation indicating potential factors affecting FT classification accuracy, including large precipitation events, extensive open water bodies, and complex terrain (Kim et al., 2017a).

Text S3. Data processing

All MODIS tiles covering the ABoVE domain were spatially mosaicked and reprojected using drop-in-bucket averaging from the 500 m native sinusoidal projection to the 6-km polar EASE-Grid 2 projection format (Brodzik et al., 2014) consistent with the AMSR FT record. The MODIS SCE and BSA records were processed by averaging high quality pixels (quality flag = 0 or 1 for SCE; quality flag = 0 for BSA) within each 6-km polar EASE-Grid cell to reduce the effects of cloud or cloud shadow contamination, and large sensor view angles. The MODIS SCE collection 6 (C6) record used the full range of NDSI (Normalized Difference Snow Index) values to minimize snow cover detection errors on the global scale (Hall Riggs and Hall, 2015), as compared to the earlier collection 5 record, which used a SCE threshold map (Hall, 2015). The MODIS SCE C6 product provides overall cloud mask improvement and better snow cover detection ability in forests and mountain regions during spring and summer (Hall, 2015; Masson et al., 2018). The MODIS SCE records from both Terra and Aqua satellites (hereafter denoted as MODIS) were combined to provide an increased number of daily snow cover observations. If resampled high quality SCE data were available from both MODIS Terra and Aqua records, the daily value was determined by averaging both SCE records. If only a single data record was available, this was used for the SCE daily value. If high-quality data were not available from either the resampled MODIS Terra or Aqua data records, the daily SCE value was defined as missing. The daily MODIS BSA value was also defined as missing when high-quality data were unavailable within a given 6-km cell. The 25 km AVHRR CDR R_{sdn} data were re-projected to the 6-km spatial grid using a nearest-neighbor resampling method. Lastly, the satellite and WMO station records were used to evaluate spatial and seasonal variations in snowpack conditions for the (2015-2016) study period.

Text S4. Major biome classification method

An ancillary map of principal climate zones was used to define dominant biomes within the ABoVE domain, and was resampled to the 6-km polar EASE-Grid 2 format (Fig. S1). The principal climate zones include 18 distinct climate-biome classifications derived by the

Scenario network for Arctic Planning and the EWHALE lab at the University of Alaska (SNAP, 2012). The biome classifications used in this investigation were derived by various climate inputs, including mean monthly temperature, total monthly precipitation, seasonality of precipitation in relation to temperature (likely snowfall vs likely rainfall), and length of non-frozen season (SNAP, 2012). We chose this map because the definition of biomes based on climate variables is more suitable for classifying the two major biomes within our study domain than other available global land cover classifications. For example, the MODIS IGBP global land cover (LC) classification is effective for distinguishing general land cover classes including shrubland, grassland, deciduous broadleaf and evergreen needleleaf forests. However, the MODIS LC data do not clearly distinguish boreal forest and arctic tundra within the ABoVE domain (SNAP, 2012). For this investigation, we aggregated the 18 climate-biomes (Table S1) to represent more general arctic tundra (Zone 1-5) and boreal forest (Zone 6-16) categories (Fig. S1), which were used to distinguish the two major ABR biomes within the study domain.

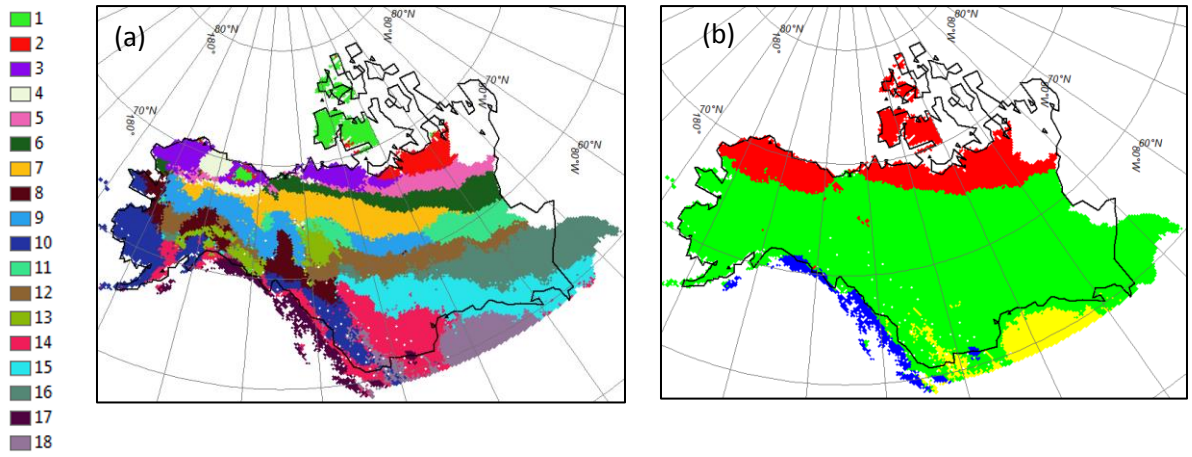

Figure S1. (a) Principal climate zones in the ABoVE study domain obtained from the Predicting Future Potential Climate-Biomes (PFPC-B) database, prepared by the Scenarios Network for Arctic Planning (SNAP) and the EWHALE lab at the University of Alaska Fairbanks (https://www.snap.uaf.edu/attachments/CliomesFINAL.pdf); (b) Four general biomes were aggregated from the larger set of 18 Alaska-Canada Climate-Biome classes and included arctic tundra (red), boreal forest (green), maritime (blue), and prairie/grassland (yellow) categories. The general categories were then used to delineate arctic tundra and boreal forest biomes within the ABoVE domain for this study. Black lines denote the ABoVE extended domain, which was used for this study. The 18 climate-biome classifications are defined in Table S1, which were used to define arctic tundra (Zones 1-5) and boreal forest (Zones 6-16) categories for this study.

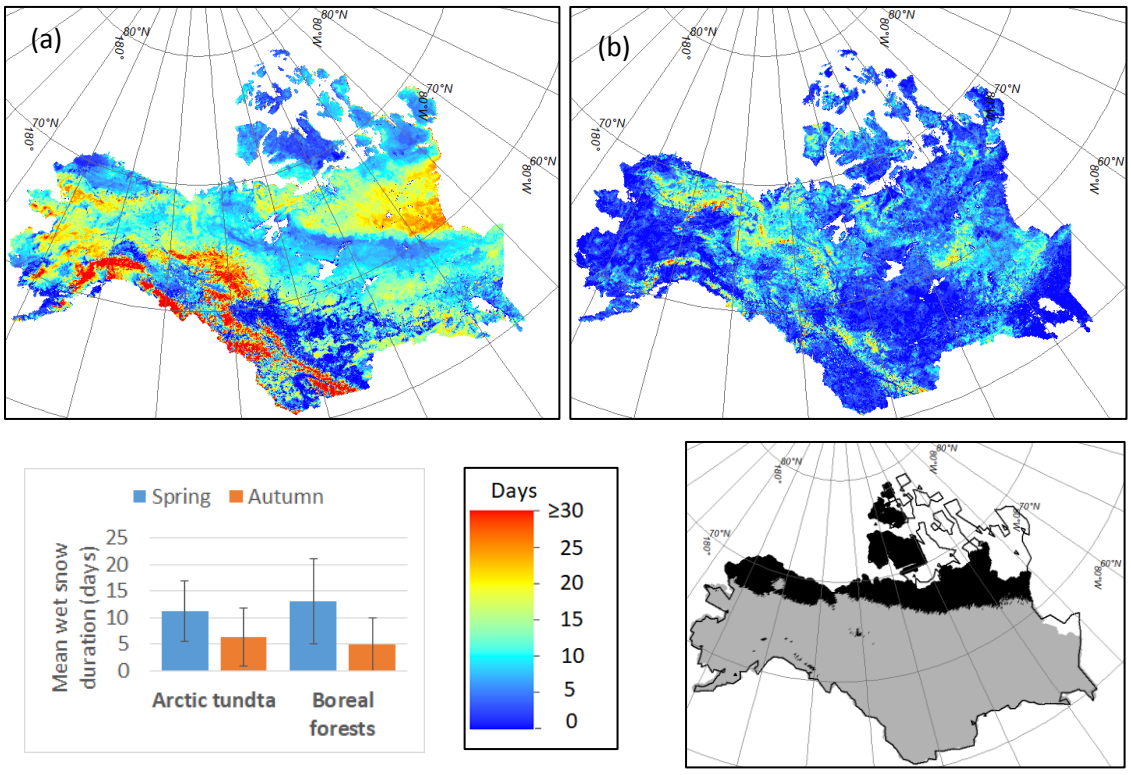

Figure S2. Spring (a) and autumn (b) wet snow duration (days) derived from the combined MODIS SCE and AMSR FT records for 2016. Black and grey areas on the inset image denote respective Arctic tundra and boreal forest biomes. The adjacent bar chart shows the mean ± SD wet snow duration during spring and autumn transitions for the tundra and boreal forest biomes.

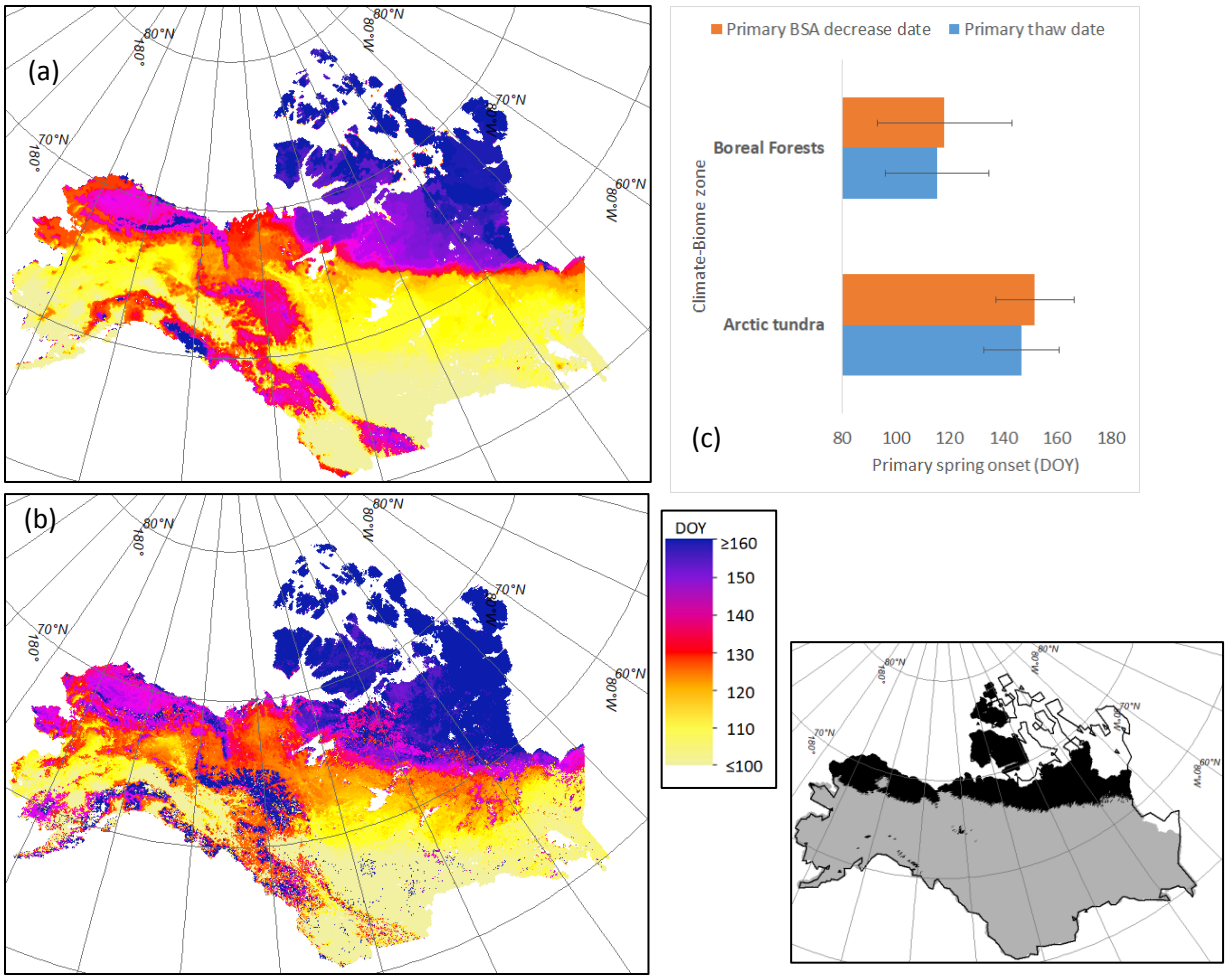

Figure S3. Primary spring onset (DOY) within the ABoVE domain for 2016 derived from the (a) AMSR FT primary thaw date and (b) MODIS BSA primary decrease date; the bar graph (c) shows the spatial mean ±SD BSA decease and primary thaw dates for the arctic tundra and boreal forest biomes. The inset map (lower right) denotes the Arctic tundra (black) and boreal forest (grey) biomes.

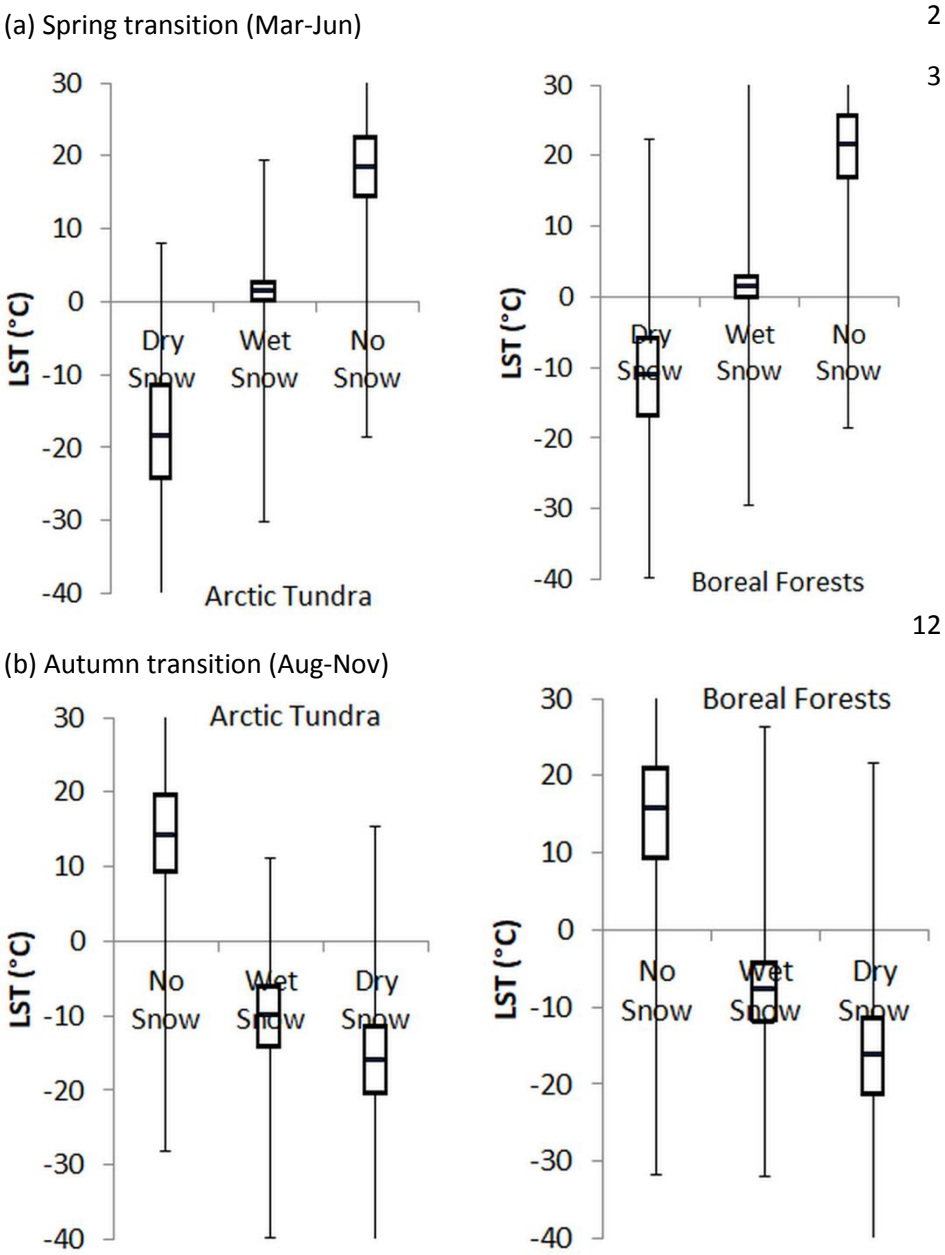

Figure S4. The distribution of mid-day land surface temperature (LST) observations from MODIS Aqua (MYD11A1) during satellite derived dry snow, wet snow and snow-free conditions over (a) spring (Mar – Jun) and (b) autumn (Aug-Nov) transition periods for arctic tundra and boreal forest biomes within the ABoVE domain from 2015-2016. All MYD11A1 tiles covering the ABoVE domain were spatially mosaicked and reprojected using drop-in-bucket averaging from the 1 km native sinusoidal projection to the 6-km polar EASE-Grid 2 projection format. The MYD11A1 LST records were processed by averaging high quality pixels (quality flag = 0) within each 6-km polar EASE-Grid cell. The box plot represents the upper (75th percentile), median (middle line) and lower (25th percentile) quartiles. The vertical lines denote minimum and maximum values.

Table S1. The 18 climate-biome classifications from the PFPC-B SNAP database.

No.	Principal climate zone description
1	Northern Arctic sparsely vegetated tundra with up to 25% bare ground and ice, with an extremely short growing season.
2	Cold northern arctic tundra, but primarily vegetated
3	More densely vegetated arctic tundra with up to 40% shrubs but no tree cover
4	Arctic tundra with denser vegetation and more shrub cover including some small trees
5	Dry sparsely vegetated southern arctic tundra
6	Northern boreal/southern arctic shrubland, with an open canopy
7	Northern boreal coniferous woodland, open canopy
8	Dry boreal wooded grasslands — mixed coniferous forests and grasses
9	Mixed boreal forest
10	Boreal forest with coastal influence and intermixed grass and tundra
11	Cold northern boreal forest
12	More densely forested closed-canopy boreal
13	Sparsely vegetated boreal with elevation influences
14	Densely forested southern boreal
15	Southern boreal/aspen parkland
16	Southern boreal, mixed forest
17	Coastal rainforest, wet, more temperate
18	Prairie and grasslands

Table S2. Distribution of BSA and R_{snet} derived from the AVHRR and MODIS data records during spring (Mar – Jun) and autumn (Aug – Nov) transitions in arctic tundra and boreal forest portions of the ABoVE domain from 2015-2016.

Spring	Stats.	arctic tundra			boreal forest		
		Dry snow	Wet snow	No snow	Dry snow	Wet snow	No snow
BSA [unitness]	Q1	0.71	0.49	0.12	0.36	0.30	0.09
	Median	0.76	0.59	0.13	0.47	0.39	0.10
	Q3	0.79	0.68	0.16	0.61	0.48	0.11
	Mean	0.73	0.58	0.15	0.49	0.40	0.11
	SD	0.09	0.12	0.07	0.16	0.13	0.04
R_{snet} [$MJ/m^2/day$]	Q1	6.16	12.57	38.56	9.65	18.26	43.98
	Median	8.80	19.13	51.25	15.59	26.62	55.21
	Q3	11.72	25.90	53.38	22.43	32.97	60.87
	Mean	9.39	19.53	44.91	16.59	25.74	50.87
	SD	15.32	29.91	39.58	29.43	34.16	36.67
Autumn	Stats.	arctic tundra			boreal forest		
		No snow	Wet snow	Dry snow	No snow	Wet snow	Dry snow
BSA [unitness]	Q1	0.12	0.33	0.37	0.09	0.25	0.25
	Median	0.14	0.41	0.54	0.10	0.31	0.31
	Q3	0.15	0.54	0.66	0.12	0.38	0.39
	Mean	0.14	0.43	0.52	0.11	0.32	0.34
	SD	0.04	0.15	0.17	0.03	0.13	0.14
R_{snet} [$MJ/m^2/day$]	Q1	17.67	3.67	2.64	18.17	3.70	3.20
	Median	27.30	6.23	4.17	30.07	5.89	5.20
	Q3	37.52	9.16	6.46	42.91	9.07	7.79
	Mean	27.72	6.92	4.90	30.94	6.96	5.88
	SD	42.29	15.27	11.12	51.63	17.04	14.03

Q1 and Q3 denote first and third quartiles, respectively. SD denotes standard deviation.

Supplementary References

Andre, C., C. Ottle, A. Royer, and F. Maignan. 2015. Land surface temperature retrieval over circumpolar Arctic using SSM/I-SSMIS and MODIS data. Remote Sensing of Environment, 162, 1-10

Bateni, S. M., C. Huang, S. A. Margulis, E. Podest, and K. McDonald. 2013. Feasibility of Characterizing snowpack and the freeze-thaw state of underlying soil using multifrequency active/passive microwave data. *IEEE Transactions on Geoscience and Remote Sensing*. 51 (7), 4085-4102

Brodzik, M. J., B. Billingsley, T. Haran, B. Raup and M. H. Savorie. 2014. Correction: Brodzik, M. J. et al. EASE-Grid 2.0: Incremental but significant improvements for Earth-Gridded Data sets. *ISPRS International Journal of Geo-Information*, 3 (3), 1154-1156

Dee, D. P., Uppala, S. M., Simmons, A. J., Berrisford, P., Poli, P., Kobayashi, S., Andrae, U., Balmaseda, M. A., Balsamo, G., Bauer, P., Bechtold, P., Beljaars, A. C. M., van de Berg, I., Biblot, J., Bormann, N., Delsol, C., Dragani, R., Fuentes, M., Greer, A. J., Haimberger, L., Healy, S. B., Hersbach, H., Holm, E. V., Isaksen, L., Kallberg, P., Kohler, M., Matricardi, M., McNally, A. P., Mong-Sanz, B. M., Morcette, J.-J., Park, B.-K., Peubey, C., de Rosnay, P., Tavolato, C., Thepaut, J. N., and Vitart, F.: The ERAInterim reanalysis: Configuration and performance of the data assimilation system, Q. J. Roy. Meteorol. Soc., 137, 553–597, 2011.

Du, J., J. S. Kimball, C. Duguay, Y. Kim, and J. D. Watts. 2017. Satellite microwave assessment of Northern Hemisphere lake ice phenology from 2002 to 2015. *The Cryosphere*, 11, 47-63

Hall, D. K. 2015. VIIRS Snow cover algorithm theoretical basis document (ATBD) (https://modis-snow-ice.gsfc.nasa.gov/uploads/VIIRS_snow_cover_ATBD_2015.pdf)

Hasting, D. A., P. K. Dunbar, G. M. Elphingstone, M. Bootz, H. Murakami, H. Maruyama, H. Masaharu, P. Holland, J. Payne, N. A. Bryant, T. L. Logan, J.-P. Muller, G. Schreier, and J. S. MacDonald, GLOBE Task Team. 1999. The global land one kilometer base elevation (GLOBE) digital elevation model, version 1.0, Nat. Ocean. Atmos. Admin., Nat. Geophys. Data Center, Boulder, CO, Digital data base on the World Wide Web and CD-ROMs. [Online]. Available: http://www.ngdc.noaa.gov/mgg/toto/globe.html

Holmes, T. R. H., W. T. Crow, M. T. Yilmaz, T. J. Jackson, and J. B. Basara. 2013. Enhancing model-based land surface temperature estimates using multiplatform microwave observations. Journal of Geophysical Research: Atmosphere, 118, 577-591

Imaoka, K., M. Kachi, M. Kasahara, N. Ito, K. Nakagawa, and T. Oki. 2010. Instrument performance and calibration of AMSR-E and AMSR2, ISPRS Archives, 38 (8), 13-18

Kawanishi, T. J., T. Sezai, Y. Ito, K. Imaoka, T. Takashima, Y. Ishido, A. Shibata, M. Miura, H. Inahata, and R. W. Spencer. 2003. The advanced scanning microwave radiometer for the

EarthObserving System (AMSR-E): NASDA's contribution to the EOS for global energy and water cycle studies. *IEEE Transactions on Geoscience and Remote Sensing*, 41 (2), 184-194

Kim, Y., J. S. Kimball, J. Glassy, and K. C. McDonald. 2018. MEaSUREs Northern Hemisphere Polar EASE-Grid 2.0 Daily 6 km Land Freeze/Thaw Status from AMSR-E and AMSR2, Version 1. Boulder, Colorado USA. NASA National Snow and Ice Data Center Distributed Active Archive Center. doi: http://dx.doi.org/10.5067/WM9R9LQ2SA85

Kim, Y., J. S. Kimball, J. Glassy, and J. Du. 2017a. An Extended Global Earth System Data Record on Daily Landscape Freeze-Thaw Status Determined from Satellite Passive Microwave Remote Sensing. *Earth System Science Data*, 9 (1), 133-147

Kim, Y., J.S. Kimball, & J. Du. 2017b. Chapter 8. Satellite Microwave Remote Sensing of Landscape Freeze-Thaw Status Related to Frost Hazard Monitoring, In Remote Sensing of Hydro-meteorological Hazards. CRC Press.

Kim, Y., Kimball, J. S., McDonald, K. C., and Glassy, J.: Developing a global data record of daily landscape freeze/thaw status using satellite passive microwave remote sensing, IEEE T. Geosci. Remote, 49, 949–960, 2011.

Masson, T., M. Dumont, M. D. Mura, P. Sirguey, S. Gascoin, J. Dedieu, and J. Chanussot. 2018. An assessment of existing methodologies to retrieve snow cover fraction from MODIS data. Remote Sensing, 10, 619

Riggs. G. A., and D. K. Hall. 2015. MODIS snow products collection 6 user guide (https://nsidc.org/sites/nsidc.org/files/files/MODIS-snow-user-guide-C6.pdf).

SNAP. 2012. Predicting Future Potential Climate-Biomes for the Yukon, Northwest Territories, and Alaska (https://www.snap.uaf.edu/attachments/Cliomes-FINAL.pdf)